Supporting Information

A Biomimetic Strip for Standardized Evaluation of Herbicide Deposition Dynamics

Zidong Zhan,[a,b] Jie Ma,[a,b] Zhuoxing Liu,[a,b] Jia Peng,[a,b] Xuan Guo,[a,b] Guanqiu Qian,[a,b] Shijie Liu,[c] Bo Wang,*[c] Cunlong Yu,*[a,c] and Zhichao Dong*[a,b,c]

a Laboratory of Bio-inspired Materials and Interfacial Science, Technical Institute of Physics and Chemistry, Chinese Academy of Sciences, Beijing 100190, China.
b School of Future Technology, University of Chinese Academy of Sciences, Beijing 100049, China.
c State Key Laboratory of Bioinspired Interfacial Materials Science, School of Nano Science and Technology, Suzhou Institute for Advanced Research, University of Science and Technology of China, Suzhou 215123, China.

Supplementary note

Methods

Materials. Plant materials comprised selected grass species provided by the National Engineering Research Center of Herbicides (NanKai University, China). Additional specimens were cultivated in the laboratory (TIPC, CAS) with seeds procured from certified online horticultural suppliers. The primary agrochemical formulation was a commercial 41 wt% glyphosate isopropylamine salt formulation purchased (Roundup, Monsanto Company, USA). A non-ionic silicone surfactant (Momentive Performance Materials (Nantong) Co., Ltd., China) was used as an adjuvant to regulate the surface tension of test droplets. The foundational substrate of the biomimetic strip was a commercial polyethylene condensation management film (3M94502, USA). Tetrachlorosilane (TCS) and octadecyltrichlorosilane (OTS) were purchased from Innochem, China, and were used for preparation of the super-repellent coating.

Plant leaf sample preparation and experimental protocol. Leaf samples of Zea mays were collected at the trefoil stage, while leaves of all other grass species were harvested at the flowering stage. Following collection, leaves were rinsed with deionized water to remove surface contaminants and subsequently dried under a gentle stream of nitrogen gas. Processed samples were stored at 4℃ prior to subsequent observation and testing experiments to preserve their native surface properties. For each species, a minimum of three individual leaves were selected to account for biological variability. To minimize post-harvest alterations in surface wettability, all experiments, including droplet impact tests, were conducted within 3 hours after leaf collection. Each sample was set with at least 5 measurement sites for data collection to ensure statistical reliability. For large-sized leaves, we selected the widest area in the middle of the leaves and cut into a standard strip (5 mm×20 mm). Leaf morphology was photographed using a digital camera (TG5, Olympus, Japan).

Environmental scanning electron microscopy (ESEM) of plant leaves. To preserve the near-native state of the leaf surface under vacuum conditions, a cryo-stabilization protocol was employed prior to the ESEM observation (QUANTA FEG 250, FEI, USA). Selected leaf samples were cleaned and then rapidly cryo-fixed by immersion in liquid nitrogen for 10 seconds and quickly mounted on the ESEM sample stage to minimize structural softening after thawing. High-resolution electron images of the leaf surface microstructures were acquired with an accelerating voltage of 10 kV. Energy-dispersive X-ray spectroscopy (EDS) for elemental analysis was performed using the same instrument (Quanta FEG 250) under identical operational parameters.

Characterize Wettability. Static contact angles were measured using a standard sessile drop method with an OCA 20 goniometer (DataPhysics Instruments GmbH, Germany). Droplets of 3.0 μL were dispensed onto the sample surface, and the equilibrium contact angle was determined from the captured droplet profile. To obtain a more comprehensive and operator-independent measurement of surface wettability, three-dimensional (3D) static contact angles were characterized using the Ayríís system (KRÜSS GmbH, Germany).

Kinetic contact tension (KCT) measurement. KCT was derived from direct adhesion force measurements quantified using a high-resolution piezoelectric force sensor (DCAT21, Dataphysics, Germany) with the resolution of 0.5 μN and sampling rate of 50 Hz. All measurements were conducted under controlled environmental conditions (20 ± 0.5°C and 30 ± 2% RH). Test droplets were suspended under a 3D-printed disc probe. Meanwhile, natural leaf samples or artificial samples were positioned on a lifting platform directly below the disc probe. During each test, samples were first raised to contact with the test droplet and compressed to a predefined strain (ε). Subsequently, the samples were descended at a constant velocity inducing the contact line retraction. The normal force (F) was recorded throughout this process. The stage height (H) was defined as zero at the point of maximum compression. During the contact line retraction phase, the normal force decreased linearly with H. KCT was thus defined as the absolute slope of this linear relation: $\mathrm{KCT} = |\mathrm{d}F/\mathrm{d}H|$.

Characterization of Droplet Impact by KCT. During droplet impact, we calculated the restitution coefficient e as $(H_1 / H_0)^{0.5}$, where H_0 and H_1 are the height of droplet before and after impact, respectively. the energy dissipation $\Delta E / E_0$ is correlate to the restitution coefficient e, where ΔE is the energy dissipation, E_0 is the initial energy, and there is: $\Delta E / E_0 = 1 - e^2$. Based on that, we use KCT to estimate the rebound velocity U_1. To account for substrate structure effects on contact time, we define the normalized normal force duration as $\lambda = t_{re} / t_r$, where t_{re} and t_r are the retraction time and the time of receding state, respectively. Previous research10 established that rebound velocity is related to the θ_{DRCA}. Incorporating contact time effects, we derive: $U_1 \sim \lambda^{0.5} (1 - \cos\theta_{DRCA})^{0.5} U_0$, where U_0 is the impact velocity. Therefore, the restitution coefficient e is estimated as: $e \sim \lambda^{0.5} (1 - \mathrm{KCT} / \gamma)^{0.5}$. We demonstrate e increases with $\lambda^{0.5} (1 - \mathrm{KCT} / \gamma)^{0.5}$ by a slope of 0.13.

Calculate the Boundary of Wenzel and Cassie States Divided by KCT. We analyze the boundaries of Wenzel and Wenzel-Cassie states divided by KCT. We begin with the relation $e \sim \lambda^{0.5} (1 - \mathrm{KCT} / \gamma)^{0.5}$. When $\mathrm{KCT} > \gamma$, the droplet fails to rebound, and thus KCT ~ 70 mN m^{-1} for water or KCT ~ 45 mN m^{-1} for 0.2% glyphosate isopropylamine salt are the boundary that determines whether it rebounds or in the Wenzel state. Then, we consider the boundary of Cassie and

Wenzel-Cassie state. We proved that KCT/γ ~ ($\sin\theta_{DRCA}$ + ($\pi - \theta_{DRCA}$) $\cos\theta_{DRCA}$) f_s, where θ_{DRCA} is the dynamic receding contact angle during KCT measurement, and f_s is the solid fraction. Due to the grass leaves have similar cuticle waxes and nanostructures, θ_{DRCA} is similar. When f_s = 1, KCT ~ 10 mN m^{-1}, Therefore, the boundary is KCT ~ 10 mN m^{-1}.

Fabrication of the biomimetic test strip. The biomimetic strip was fabricated using a commercially available 3M94502 polyethylene condensation management film as the structured substrate. The film was cut into strips of the desired size, and the structured side was used as the coating surface. A superhydrophobic coating precursor was prepared by dissolving TCS (4% w/v) and OTS (2% w/v) in anhydrous petroleum ether under dry conditions. The precursor solution was then applied uniformly onto the structured side of the 3M film by brush coating. After coating, the samples were left under ambient conditions to allow hydrolysis and condensation of the chlorosilanes, forming a nanoscale silica/siloxane network physically anchored to the substrate.

High-resolution micro-computed tomography (Micro-CT) Imaging of plant leaf topology. To preserve the native three-dimensional microstructure, cleaned plant leaves were sandwiched between water-saturated sponges to prevent dehydration and deformation during scanning. The sample assembly was mounted on the stage of a Micro-CT scanner (Skyscan 1272, Bruker, USA). The setup was enclosed with a transparent cover and sealed with parafilm to minimize evaporation. Each scan was performed at a 4K resolution to obtain detailed volumetric data of the leaf venation architecture.

Quantitative surface topography analysis. Surface topography was characterized using a 3D optical microscope (DSX 1000, Olympus, Japan). Leaf samples were firmly adhered to glass slides to ensure stability during imaging. To ensure consistency, the analysis area was selected between two adjacent lateral veins. Images were acquired at 320× magnification. From the reconstructed 3D surface maps, key areal roughness parameters—including the root-mean-square height (Sq) and the arithmetic mean height (Sa)—were calculated to quantify topographic complexity

High-speed droplet impact experiment. Droplets were released from a predetermined height *via* the peristaltic pump (Longer TSA-1A, China) to control impact velocity upon the substrate. Droplet diameter was preset as 1.1 mm. Imaging was performed perpendicular to the leaf vein direction to clearly capture the contact line motion and avoid obstruction by veins. For standard experiment, the droplet was released from 5 cm height (1m s^{-1}). The droplet impact process was recorded using a high-speed camera (NOVA S20, FASTCAM, Japan) at a frame rate of 10000 fps.

Supplementary Figures

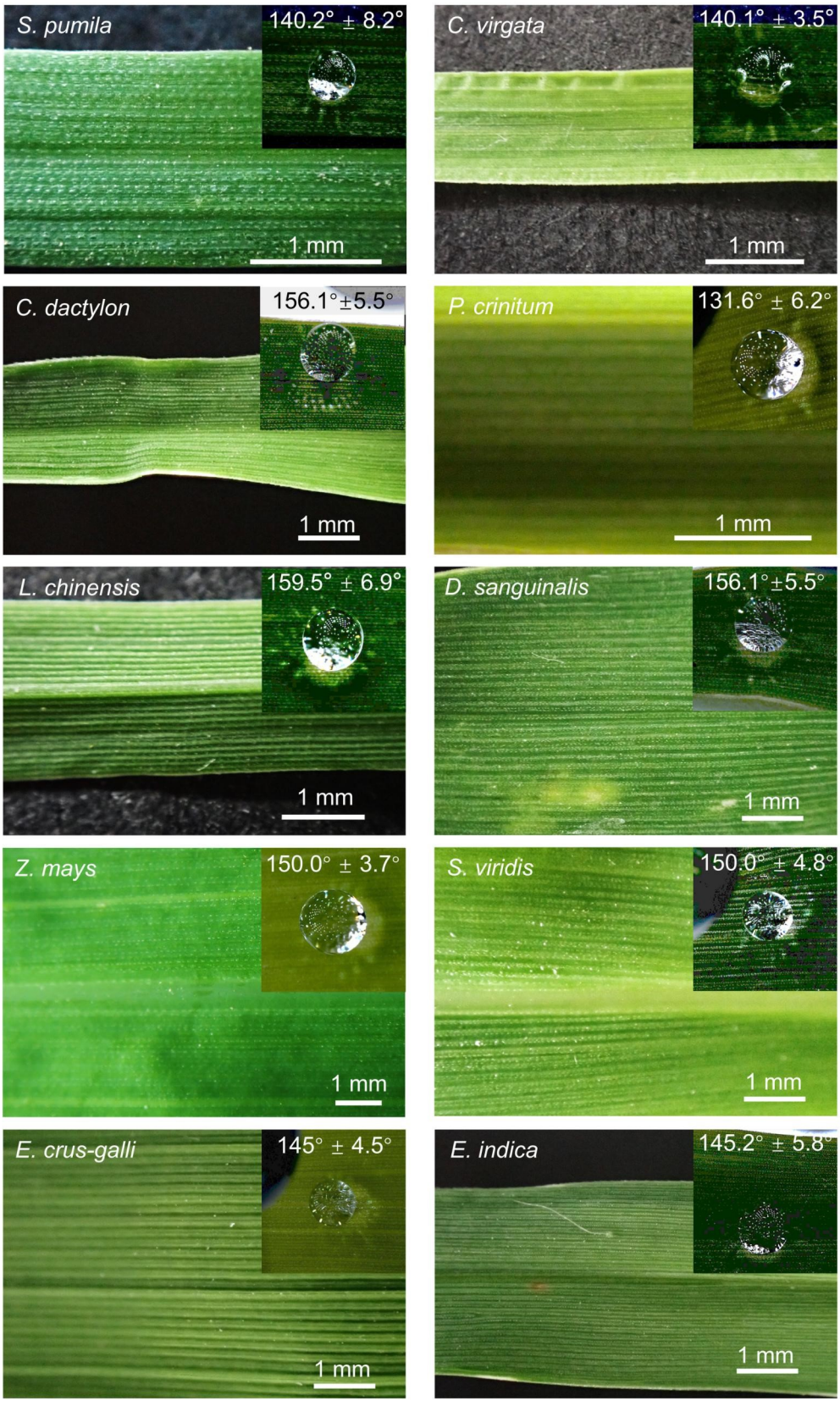

Fig. S1 Surface morphology and correlated static contact angles of selected C4 grass species.

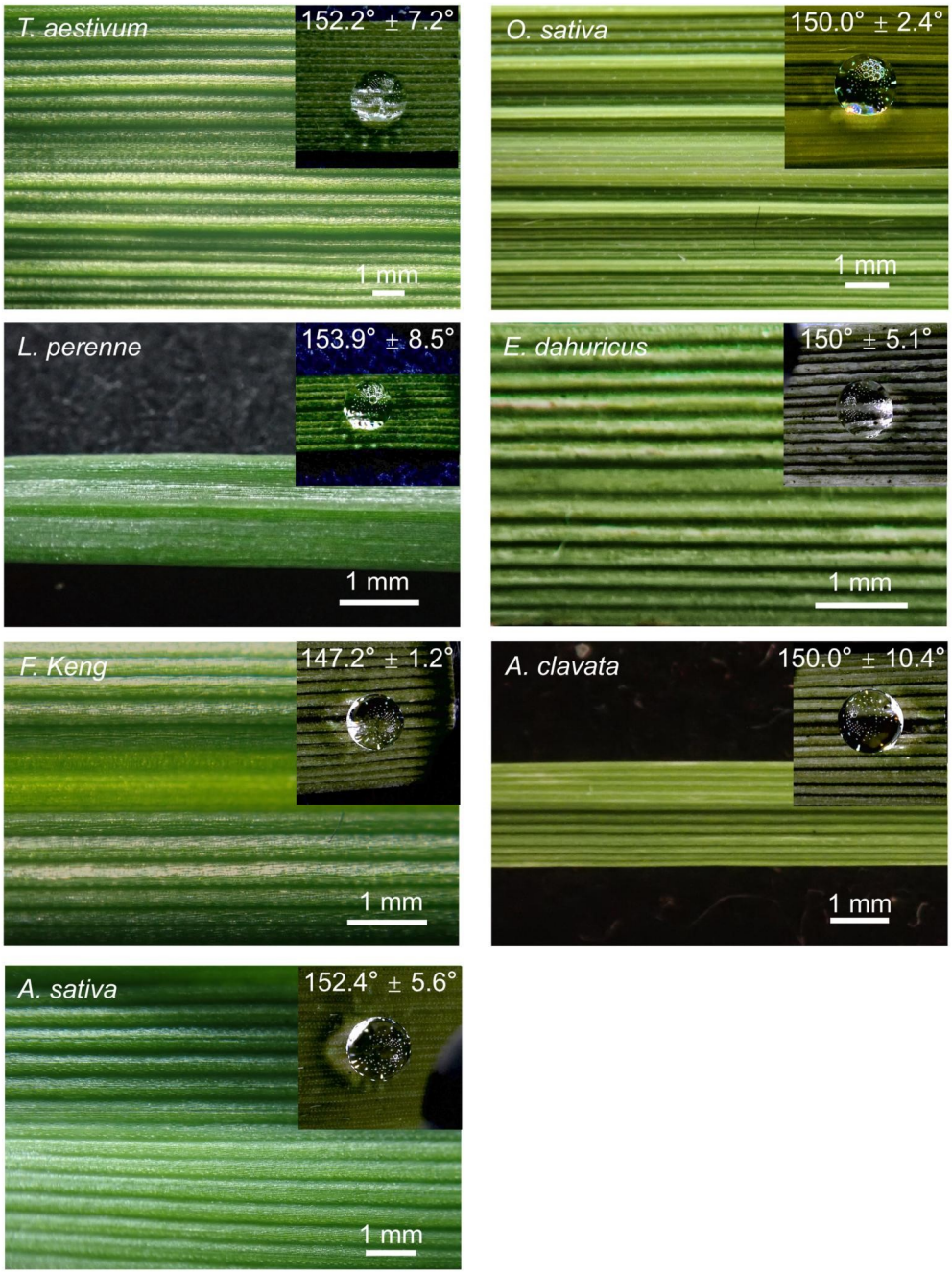

Fig. S2 Surface morphology and correlated static contact angles of selected C3 grass species.

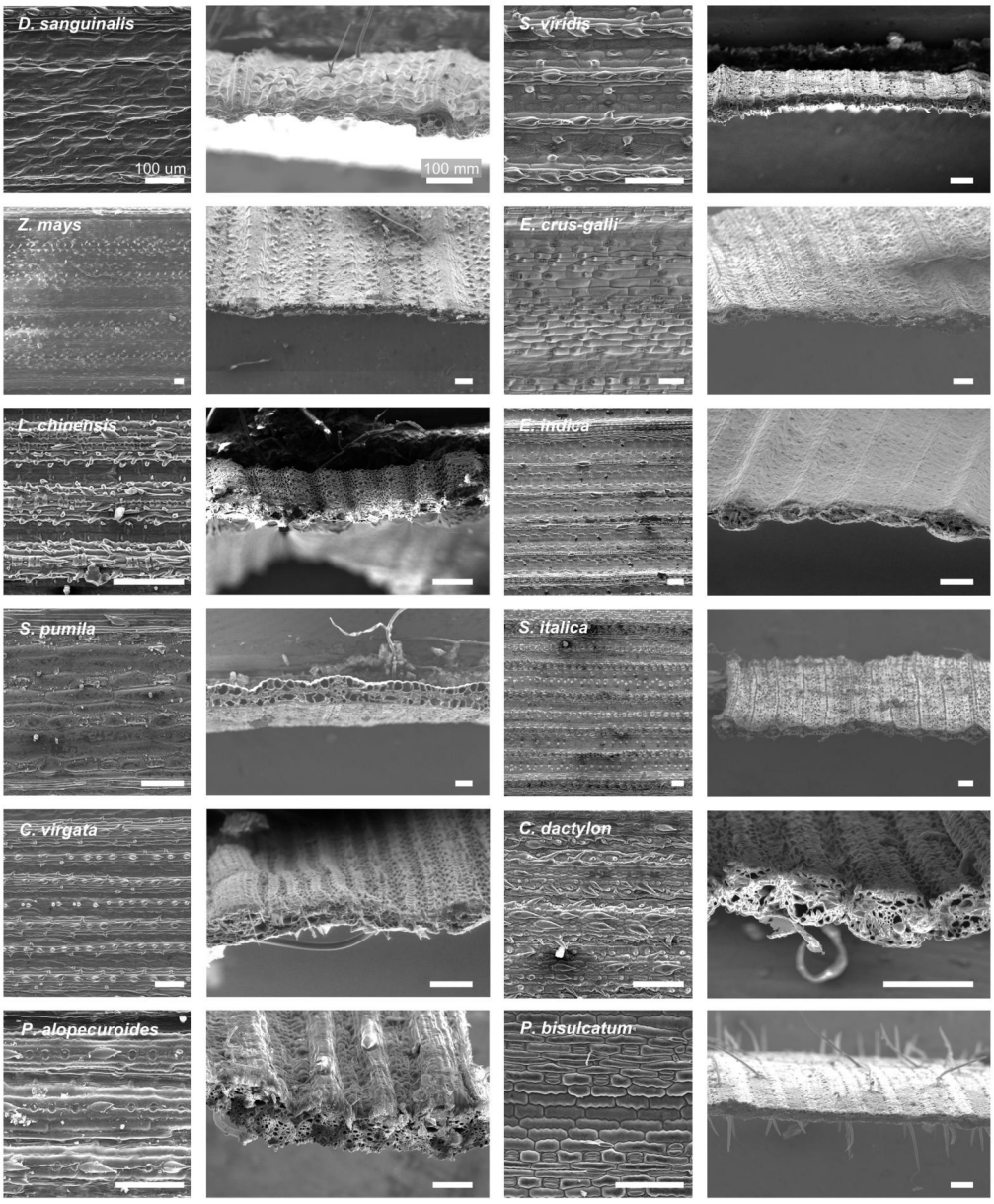

Fig. S3 SEM micrographs of C4 plant leaf surface (top view) and cross-section.

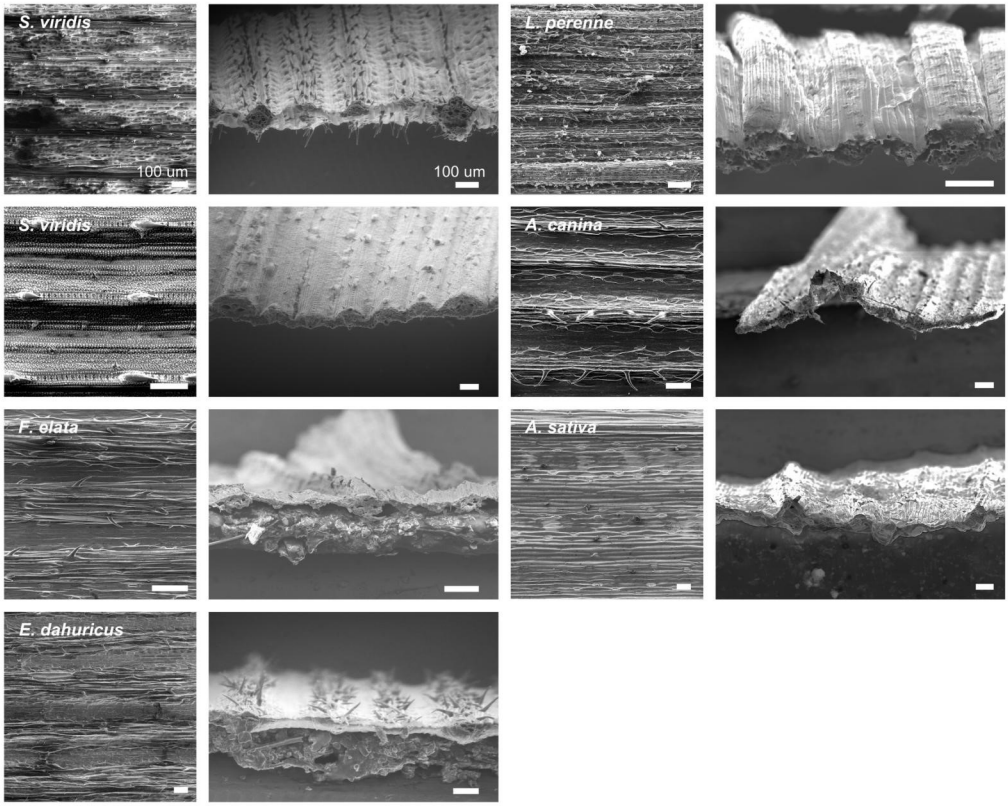

Fig. S4 SEM micrographs of C3 plant leaf surface (top view) and cross-section.

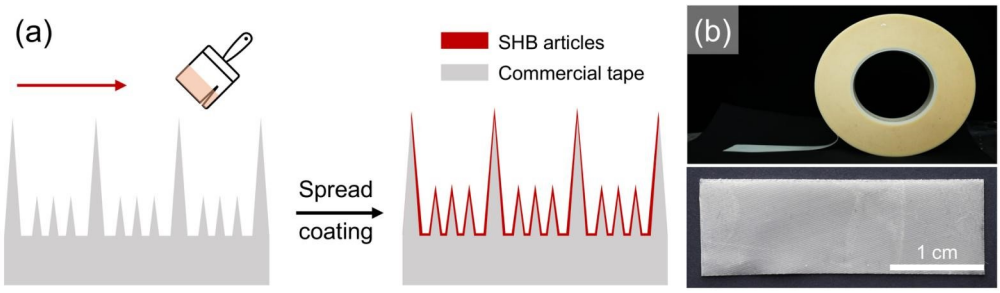

Fig. S5 Fabrication of the biomimetic test strip *via* brush-coating. (a) Schematic illustration of the brush-coating process. (b) Optical images of the fabricated strip.

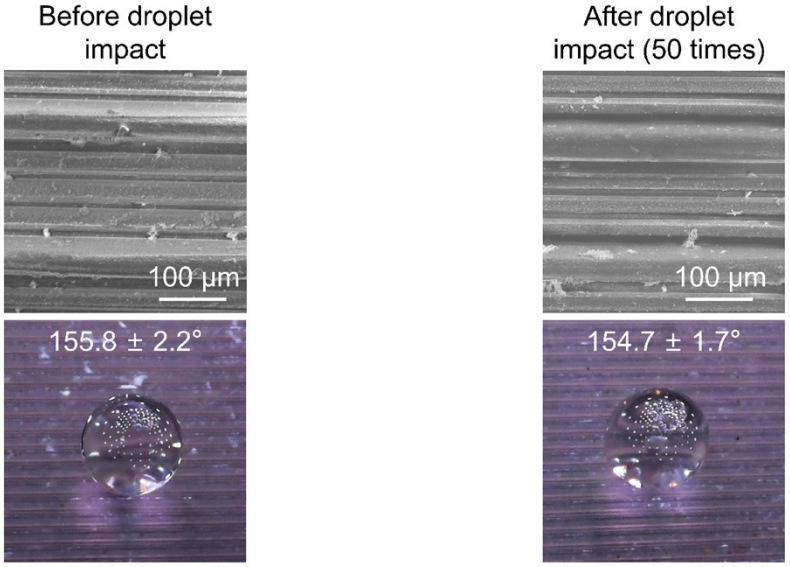

Fig. S6 Wettability and SEM characterization of the test strip after 50 droplet-impact cycles.

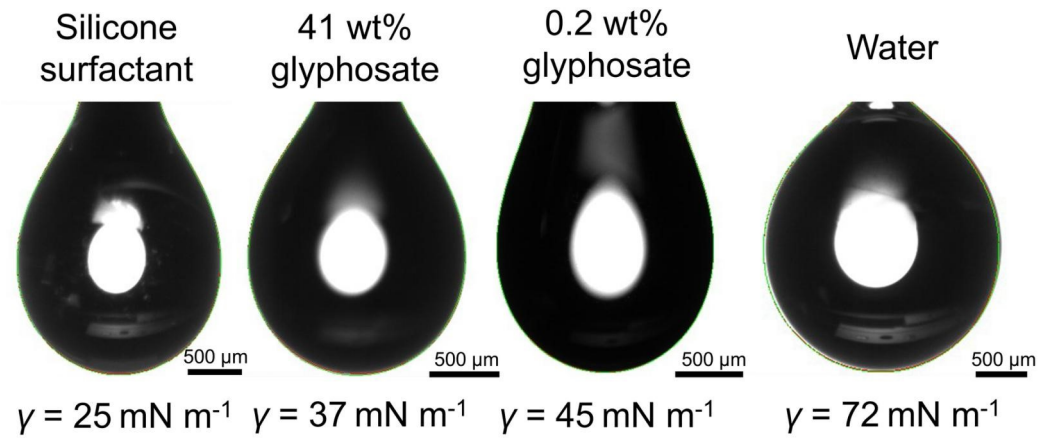

Fig. S7 Surface tension measurement *via* the pendant drop method. Values are reported for water, a silicone-based glyphosate isopropylamine salt, and 41% glyphosate isopropylamine salt at two concentrations (0.2 wt% and 41 wt%).

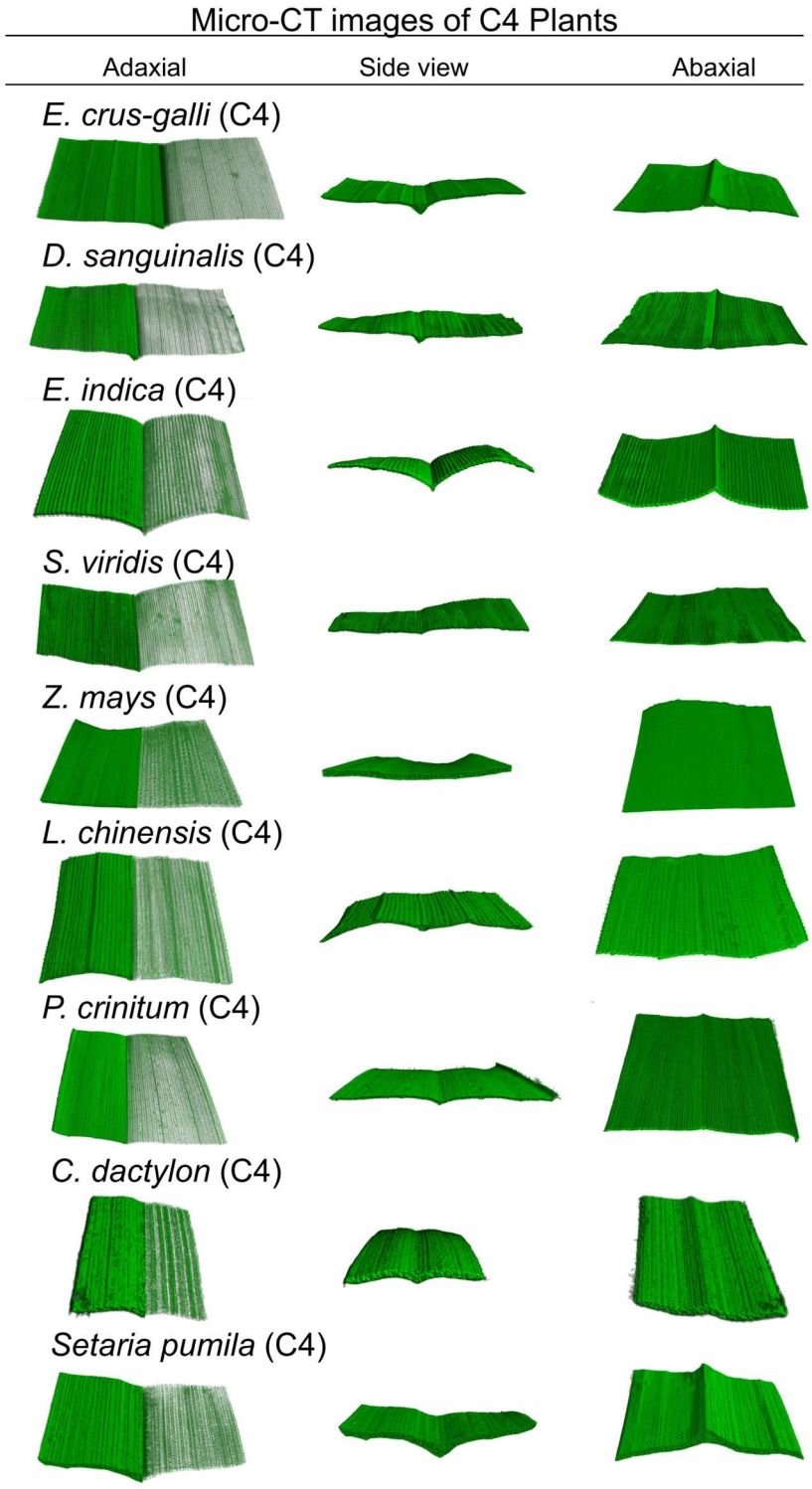

Fig. S8 3D reconstruction *via* Micro-CT scanner of leaves from nine C4 grass species.

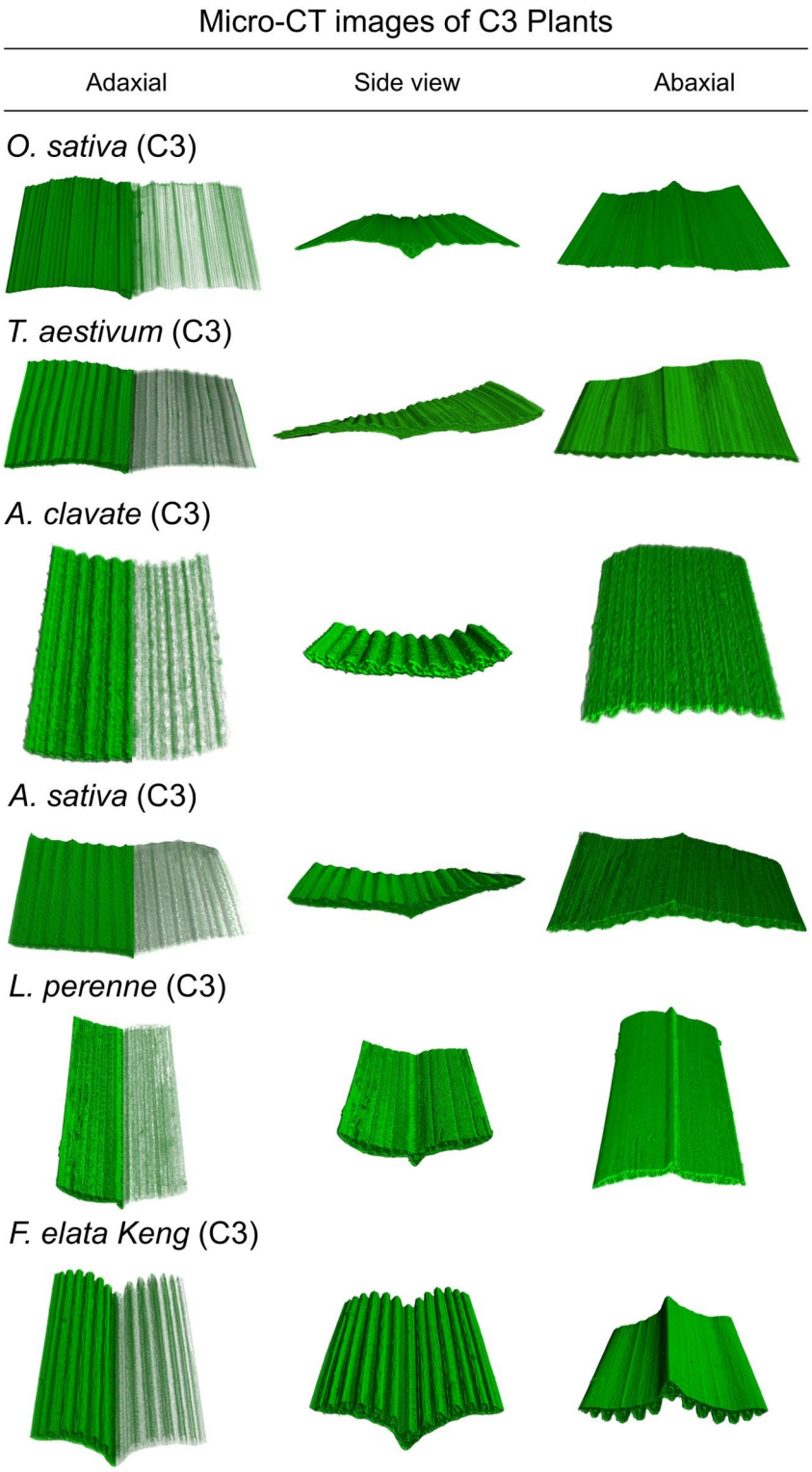

Fig. S9 3D reconstruction *via* Micro-CT scanner of leaves from six C3 grass species.

C4 Plants

Photography images	Surface topology	Roughness coefficient
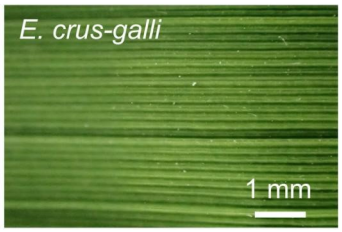	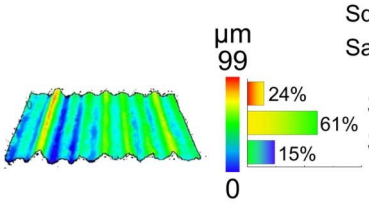	Sq: Root Mean Square Height Sa: Arithmetic Mean Height Sq = 15.2 ± 1.9 (μm) Sa = 12.1 ± 1.8 (μm)
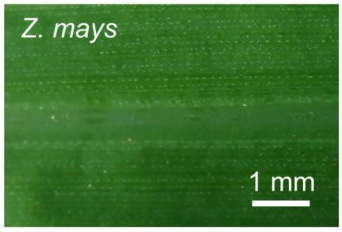	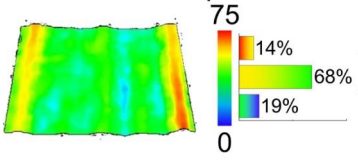	Sq = 9.6 ± 1.0 (μm) Sa = 7.6 ± 1.0 (μm)
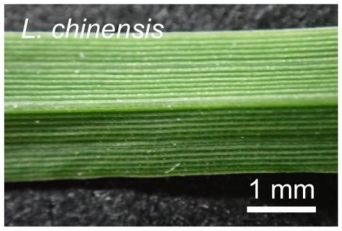	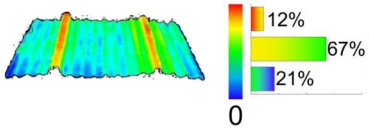	Sq = 9.6 ± 0.7 (μm) Sa = 7.2 ± 0.7 (μm)
	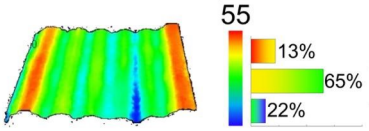	Sq = 9.5 ± 0.3 (μm) Sa = 7.6 ± 0.2 (μm)
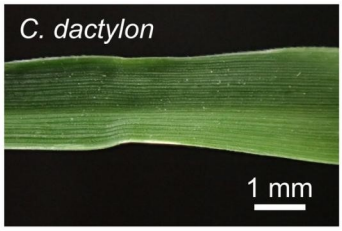	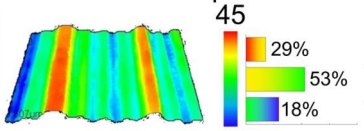	Sq = 9.0 ± 0.5 (μm) Sa = 7.3 ± 0.5 (μm)
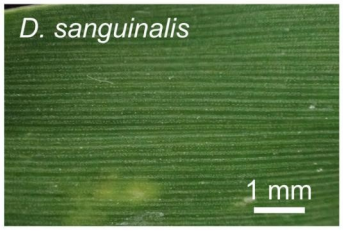	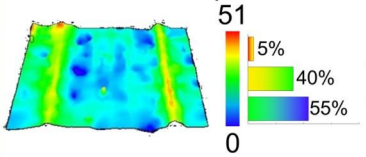	Sq = 6.4 ± 0.5 (μm) Sa = 4.8 ± 0.4 (μm)

(Continue on the next page)

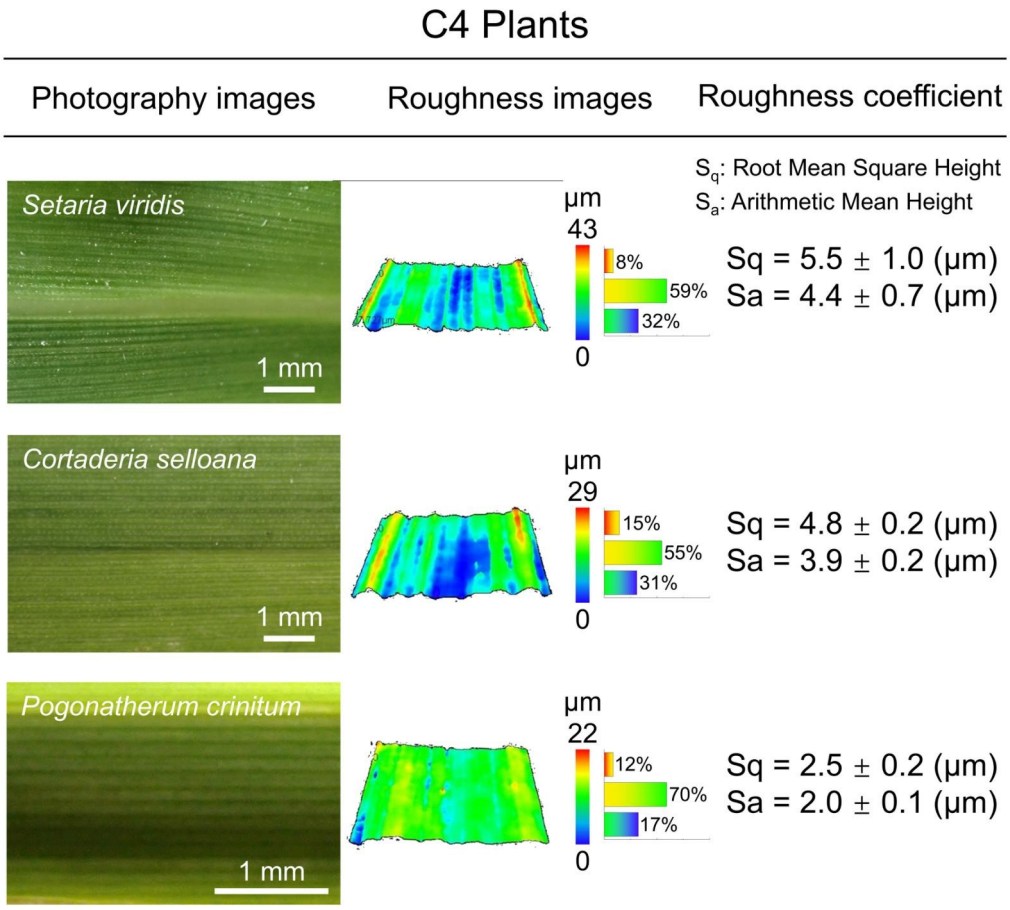

Fig. S10 Vein architecture and surface topography of nine C4 grass leaves. The analysis includes top-view optical images, corresponding surface roughness maps, and the arithmetic mean height (Sa) as a key roughness parameter.

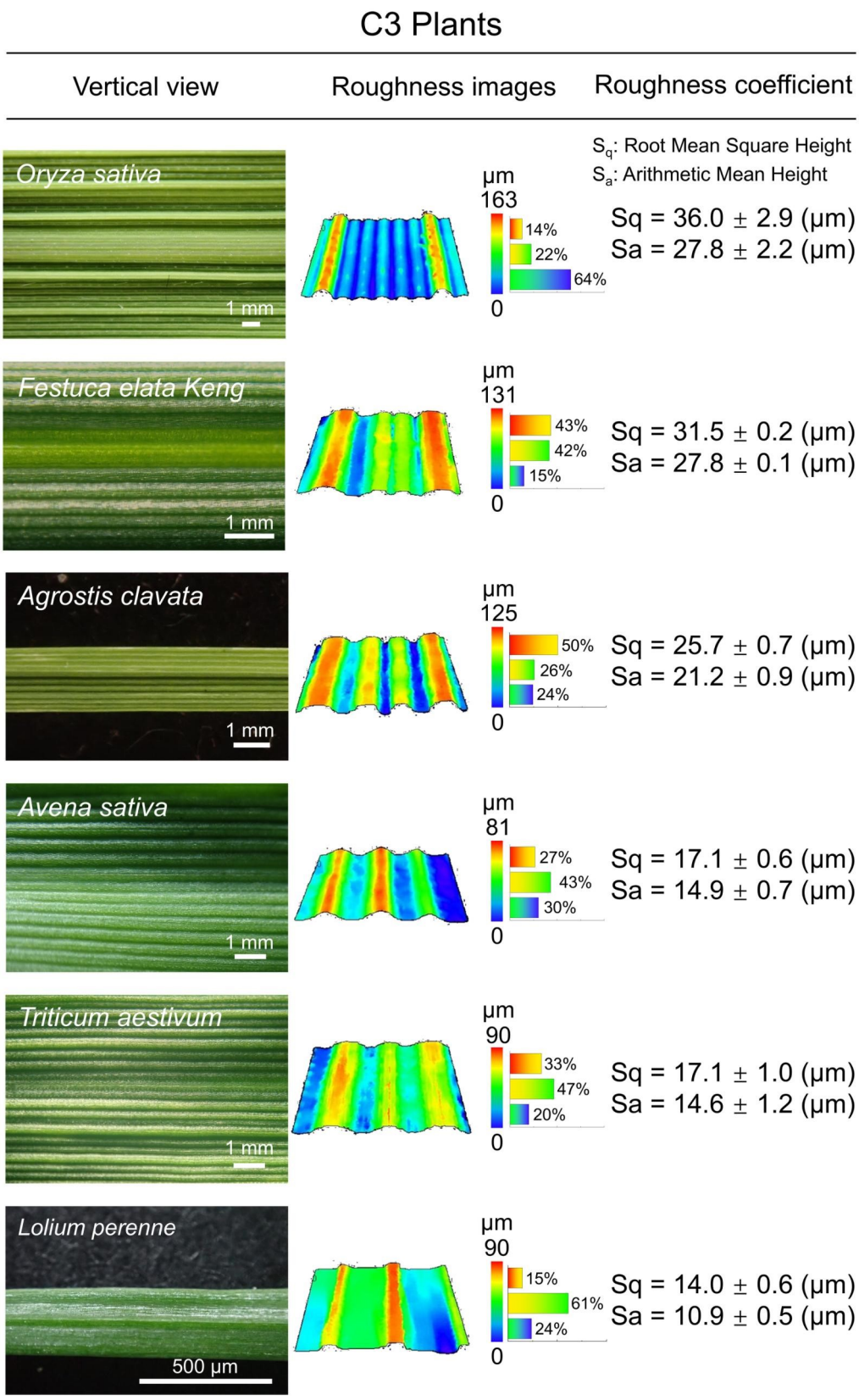

Fig. S11 Vein architecture and surface topography of six C3 grass leaves. The analysis includes top-view optical images, corresponding surface roughness maps, and the arithmetic mean height (Sa) as a key roughness parameter.

Supporting Tables

Table S1. Sampling information in 84 species of plants in nine orders

Species	*N* × *n*	Species	*N* × *n*
Ambrosia artemisiifolia	3 × 5	*Lolium perenne*	3 × 5
Artemisia annua	3 × 5	*Oryza sativa*	6 × 8
Artemisia indica	3 × 4	*Oryza sativa f. spontanea*	3 × 5
Artemisia mongolica	3 × 5	*Panicum miliaceum*	3 × 5
Aster subulatus	3 × 5	*Paspalum distichum*	3 × 5
Bidens pilosa	3 × 5	*Pennisetum alopecuroides*	3 × 7
Cichorium intybus	3 × 4	*Phragmites australis*	3 × 6
Cirsium setosum	3 × 5	*Pogonatherum paniceum*	3 × 5
Conyza canadensis	3 × 5	*Roegneria kamoji*	3 × 4
Conyza sumatrensis	3 × 5	*Setaria italica*	3 × 4
Eclipta prostrata	3 × 5	*Setaria pumila*	3 × 4
Flaveria bidentis	3 × 5	*Setaria viridis*	4 × 5
Helianthus tuberosus	3 × 5	*Triticum aestivum*	5 × 7
Lactuca serriola	3 × 5	*Typha orientalis*	3 × 7
Lactuca indica	3 × 5	*Zea mays*	3 × 5
Solidago canadensis	3 × 5	*Convolvulus arvensis*	3 × 5
Sonchus arvensis	3 × 5	*Ipomoea lacunosa*	3 × 5
Sonchus oleraceus	3 × 5	*Ipomoea purpurea*	3 × 5
Taraxacum officinale	3 × 5	*Physalis alkekengi*	3 × 4
Tripolium vulgare	3 × 5	*Brassica juncea*	3 × 5
Lamium amplexicaule	3 × 6	*Brassica oleracea*	4 × 5
Mentha haplocalyx	4 × 6	*Abutilon theophrasti*	3 × 6
Ocimum basilicum	3 × 5	*Malva sylvestris*	3 × 5
Plantago asiatica	3 × 5	*Hibiscus trionum*	3 × 5
Rehmannia glutinosa	3 × 4	*Acalypha australis*	3 × 5
Salvia elegans	4 × 6	*Euphorbia helioscopia*	3 × 5
Veronica didyma	3 × 5	*Geranium carolinianum*	4 × 6
Agrostis stolonifera	4 × 5	*Pelargonium hortorum*	3 × 6
Alopecurus myosuroides	3 × 6	*Alternanthera philoxeroides*	3 × 5
Avena sativa	4 × 5	*Amaranthus tricolor*	3 × 5
Chloris virgata	3 × 5	*Amaranthus retroflexus*	3 × 5
Cortaderia selloana	4 × 7	*Chenopodium album*	3 × 5
Cynodon dactylon	3 × 3	*Chenopodium ficifolium*	3 × 3
Digitaria sanguinalis	5 × 6	*Chenopodium glaucum*	3 × 5
Echinochloa crus-galli	6 × 8	*Chenopodiastrum hybridum*	3 × 5
Eleusine indica	4 × 5	*Dianthus barbatus*	3 × 5
Elymus dahuricus	3 × 5	*Persicaria lapathifolia*	3 × 5
Eragrostis pilosa	3 × 5	*Persicaria orientalis*	3 × 5
Festuca arundinacea	3 × 3	*Persicaria maculosa*	3 × 5
Imperata cylindrica	3 × 6	*Portulaca oleracea*	3 × 5
Leptochloa chinensis	3 × 6	*Rumex crispus*	3 × 5
Lolium multiflorum	3 × 6	*Spergula arvensis*	3 × 5

Table S2. Adhesion force and KCT of water and herbicides on the C4 leaves

Plant		Water (γ = 72 mN m^{-1})		0.2% GI (γ = 45 mN m^{-1})	
		Adhesion force (μN)	KCT (mN m^{-1})	Adhesion force (μN)	KCT (mN m^{-1})
E. crus-galli	**Adaxial**	40.8 ± 1.2	1.8 ± 1.6	68.1 ± 0.3	18.3 ± 9.5
	Abaxial	70.6 ± 8.7	2.2 ± 0.5	64.0 ± 11.0	34.5 ± 2.4
E. indica	**Adaxial**	76.0 ± 2.5	39.9 ± 4.7	84.3 ± 2.8	33.9 ± 8.4
	Abaxial	89.7 ± 8.5	50.3 ± 1.8	78.8 ± 3.0	41.4 ± 1.8
D. sanguinalis	**Adaxial**	74.8 ± 6.8	33.2 ± 3.4	87.2 ± 1.4	39.5 ± 3.3
	Abaxial	202.7 ± 5.3	128.1 ± 4.5	166 ± 11.0	103.6 ± 10.6
S. viridis	**Adaxial**	119.6 ± 8.4	58.0 ± 3.7	87.2 ± 1.4	50.8 ± 1.4
	Abaxial	190.3 ± 3.5	119.4 ± 4.1	166 ± 11.0	68.6 ± 1.3
C. virgata	**Adaxial**	62.6 ± 2.5	6.8 ± 0.7	69.6 ± 1.3	36.7 ± 5.0
	Abaxial	36.4 ± 8.4	7.1 ± 1.4	175.6 ± 8.4	106.8 ± 3.9
P. alopecuroides	**Adaxial**	102.4 ± 4.4	45.3 ± 6.5	94.9 ± 10.5	46.5 ± 4.8
	Abaxial	131.3 ± 6.8	67.0 ±7.6	105.5 ± 5.0	106.6 ± 6.3
L. chinensis	**Adaxial**	96.0 ± 1.1	7.1 ± 0.1	63.5 ± 4.4	28.5 ± 7.6
	Abaxial	49.8 ± 8.5	6.8 ±0.1	83.4 ± 3.3	32.7 ± 4.7
Z. mays	**Adaxial**	109.2 ± 4.3	6.3 ± 0.2	73.5 ± 3.0	29.9 ± 1.2
	Abaxial	69.2 ± 4.6	5.1 ±0.7	64.5 ± 4.5	37.6 ± 5.6
C. dactylon	**Adaxial**	48.9 ± 2.3	2.2 ± 1.6	120.5 ± 7.1	47.6 ± 8.8
	Abaxial	95.8 ± 15.5	65.6 ±6.4	128.5 ± 15.0	58.0 ±4.8
S. pumila	**Adaxial**	54.7 ± 7.4	50.0 ± 5.5	167.9 ± 6.5	49.4 ± 13.3
	Abaxial	227.5 ± 3.0	120.2 ±5.0	180.4 ± 16.9	113.0±18.0

Table S3. Adhesion force and KCT of water and herbicides on the C3 leaves

Plant		Water (γ = 72 mN m^{-1})		0.2% GI (γ = 45 mN m^{-1})	
		Adhesion force (μN)	KCT (mN m^{-1})	Adhesion force (μN)	KCT (mN m^{-1})
O. sativa	**Adaxial**	43.4 ± 0.9	2.1 ± 0.5	66.9 ± 5.5	18.1 ± 16.6
	Abaxial	81.0 ± 12.6	2.4 ± 0.4	100.5 ± 4.4	46.1 ± 7.1
E. dahuricus	**Adaxial**	31.0 ± 0.9	41.7 ± 5.7	91.9 ± 2.1	34.7 ± 10.4
	Abaxial	81.0 ± 12.6	94.2 ± 16.0	182.9 ± 2.2	127.0 ± 5.9
F. elata Keng	**Adaxial**	95.3 ± 13.7	42.8 ± 5.1	87.1 ± 3.0	35.0 ± 3.7
	Abaxial	174.6 ± 10.0	114.8 ± 7.8	190.3 ± 15.4	163.3 ± 12.9
A. clavata	**Adaxial**	93.7 ± 1.3	44.3 ± 2.2	91.0 ± 2.4	40.9 ± 5.7
	Abaxial	168.3 ± 10.8	90.3 ± 5.4	131 ± 6.1	62.9 ± 6.5
T. aestivum	**Adaxial**	51.5 ± 2.6	7.1 ± 2.5	96.7 ± 2.1	40.2 ± 5.4
	Abaxial	116.7 ± 3.9	90.3 ± 5.4	173.2 ± 5.4	117.1 ± 4.8
L. perenne	**Adaxial**	51.5 ± 2.6	44.3 ± 2.2	81.3 ± 4.6	40.0 ± 2.7
	Abaxial	116.7 ± 3.9	46.2 ± 7.0	84.4 ± 7.8	45.1 ± 8.9
A. sativa	**Adaxial**	83.1 ± 18.1	6.2 ± 0.6	94.2 ± 9.3	44.6 ± 3.8
	Abaxial	50.0 ± 8.5	8.7 ±1.9	211.3 ± 3.6	138.1 ± 7.0